Article

Not peer-reviewed version

Investigations on Motion Responses of Suspended Submersible in Internal Solitary Wave Field

Zhenyang He , Wenbin Wu , Junrong Wang * , Lan Ding , Qiangbo Chang , Yahao Huang

Posted Date: 11 March 2024

doi: 10.20944/preprints202403.0558.v1

Keywords: ISW fluid field; Suspended submersible; Fluid-structure interaction; Motion response

Article

Investigations on Motion Responses of Suspended Submersible in Internal Solitary Wave Field

Zhenyang He [1], Wenbin Wu [1,2], Junrong Wang [1,2,*], Lan Ding [3], Qiangbo Chang [1] and Yahao Huang [1]

[1] College of Engineering, Ocean University of China, Qingdao, 266100, China
[2] Shandong Province Key Laboratory of Ocean Engineering, Ocean University of China, Qingdao, 266100, China
[3] Fisheries Research Institute of Fujian, Xiamen, 361012, China
* Correspondence: wangjunrong@ouc.edu.cn

Abstract: While the underwater submersible encounters internal solitary wave (ISW), its loadings and motions would be seriously disturbed. To investigate the interaction effect between the suspended submersible and ISW, a three dimensional ISW-submersible interaction numerical model was established based on the Computational Fluid Dynamics (CFD) method. The generation and propagation of ISW was simulated in a two-layer fluid numerical wave tank according to the eKdV theory. The standard operation equation of submersible was introduced to simulate the six degree of freedom (6DoF) motions of submersible combined with the overset dynamic mesh method. The motion simulation method of submersible was effectively validated by comparing with published experimental results on the motion responses of the slender body under the ISW. Based on the constructed numerical model, the dynamic mechanism between the suspended submersible and ISW were studied, and the effects of the initial submerged depths and the ISW amplitudes on the dynamic responses of the submersible were revealed. According to the numerical results, the motions of the submersible have been significantly determined by its initial submerged depths. The submersible located above the ISW interface has a significant motion along the propagation direction of ISW and its motion trajectory resembles a counterclockwise semi ellipse. The motions of the submersible located below the ISW interface follows with the trace of the lower layer fluid which presented as an unclosed clockwise ellipse. The corresponding motions of the submersible would be increased as the increase of the ISW amplitudes.

Keywords: ISW fluid field; suspended submersible; fluid-structure interaction; motion response

1. Introduction

Internal solitary wave (ISW) is a kind of nonlinear fluctuation that frequently occurs in stratified ocean. Due to the small difference in vertical density, the hydrostatic recovery forces of ISW are much less than that of the free surface wave. Even a small disturbance in the stratified ocean can arouse a large amplitude nonlinear internal wave[1,2]. Besides, due to the balance between dispersion and nonlinearity effect, ISW can propagate over several hundred kilometers with stable wave shape and propagating speed. It carries huge energy in the process of propagation and causes extremely strong underwater shear currents[3–5]. Under the action of the huge ISW currents, the loadings and motions of the marine structures may be heavily disturbed. Especially for the submerged structure, it's affected by the ISW fluid field directly. In recent years, the reports of the underwater submersible crashing or even sinking while encountering ISW is not rare[6–8]. Therefore, it is necessary to carry out the investigations of the interaction mechanism between ISW fluid field and movable submersible to improve the safety and maneuverability of submersible while encountering ISW.

In order to prevent or weaken the damage of ISW to the marine structures, over the years, many scholars have carried out the experimental investigations on the interaction mechanism between the submerged or floating structures and ISW. For the floating structures, Chen et al.[9,10] performed the experimental research on the fixed semi-submersible platform under the ISW environment and

 doi:10.20944/preprints202403.0558.v1

measured the ISW loadings on the platform. Cui et al.[11] conducted the experimental studies on the moored structure and obtained the motion responses and mooring tensions of the floating structure under the action of ISW. For the submerged structure, Wang et al.[12,13] carried out the experimental studies on the interaction between ISW and fixed underwater slender body in the stratified flume and revealed the relationships between the fixed structure and the ISW fluid field. Cui et al.[14,15] recorded the real-time motion responses of the underwater structure under ISW through the experimental method, and the influence of the amplitude of ISW and fluid stratification ratio on the motion response were discussed. However, the model experiments are constrained by the scale effects. In the above mentioned experiments, the scale of the characteristic structure were intentionally enlarged in order to better measure the loadings or capture the motions of the structure which may result in some difficulties to convert the experimental results to the realistic physical background. Additionally, there are few experimental studies on the the complex structure model, and more attentions are drawn to the simple structures such as cylinders or spheres.

Considered the scale effect and high costs of the experimental method, the theoretical analysis method has gradually become an effective way to investigate interaction mechanism between ISW and structures. Cai [16–18] proposed a new method based on the ISW theory and Morison equations to calculate the ISW loadings on the simple slender cylindrical structure. Based on the above method, some scholars [19–21] simulated the motions of the structures while encounter the ISW by introducing the 6DOF motion equations of the rigid body. Besides, some scholars[22,23] investigate the interaction effect between the floating structure and ISW based on the potential theory combined with ISW equations. Although the most previous investigations of the motion simulations using mathematical model are convenient and efficient, they cannot consider the dynamic interaction effect between ISW fluid field and structure. The theory analysis method ignores the interference of the structures on fluid fields and also can not capture the generation and propagation characteristics of ISW.

Due to the aforementioned limitations of experimental method and theoretical analysis method. Recently, CFD method has been widely used to investigate numerically due to its visualization and reliability. Many scholars [24–26] established the numerical model to investigate FSI (Fluid-Structure Interaction) effect between the ISW and the fixed structure and obtained the loading history of the structure. Subsequently, some scholars [27–29] have studied the interaction characteristics between ISW and the movable structure and obtained the motion responses of the structure by applying the 6DOF calculation module of CFD software directly. However, the motion responses of the structure may be overestimated while the underwater stability of the structure is ignored, especially in the pitch direction.

Based on the experimental, theoretical or CFD numerical method, extensive investigations have been carried out to reveal the interaction effect of the underwater submersible while encountering ISW. However, most previous investigations focus on the ISW loading characteristic on fixed structure. The investigation of the motion characteristics of the movable submersible under ISW environment is still scarce. In order to further investigate the ISW-structure dynamic interaction effect, a time domain numerical model is proposed based on the secondary development of CFD software in this paper. The numerical model involved are introduced in Sections 2, the modeling and validating of the numerical model are introduced in Sections 3. In Sections 4, the effect of the initial submerged depths of submersible and the amplitudes of ISW on the motion responses of the submersible are addressed according to the numerical results. Finally, the conclusions are drawn in Section 5.

2. Numerical Theory

2.1. Basis Equations for Fluid-Structure Interaction

To simulate the motion properties of the movable submersible in the ISW fluid field, therefore, the fluids are treated as incompressible and viscous to calculate the driving forces acting on the submersible more accurately. The governing equations of ISW fluid field are the mass continuity

 doi:10.20944/preprints202403.0558.v1

equation and the Reynolds-averaged Navier-Stokes (RANS) equations[30]. They can be written as follows:

$$\frac{\partial \overline{u_i}}{\partial x_i} = 0, \tag{1}$$

$$\frac{\partial \overline{u_i}}{\partial t} + \sum_j \overline{u_j} \frac{\partial \overline{u_i}}{\partial x_j} = -\frac{1}{\rho}\frac{\partial P}{\partial x_i} + F_i + \nu \sum_j \frac{\partial^2 \overline{u_i}}{\partial x_i^2} - \sum_j \frac{\partial \overline{u_i' u_j'}}{\partial x_j}, \tag{2}$$

where $\overline{u}_i$ is the time-average velocity; u_i' represents the fluctuation velocity; F_i is the mass force; P is the pressure; ρ is the fluid density; ν is the fluid kinematic viscosity. The above fluid governing equations are numerically solved by Finite Volume Method (FVM). The turbulent viscosity of the above governing equation ν is solved by the RNG *k-ε* two equations closed model[31]. The Coupled algorithm is applied to solve the pressure velocity coupling term. Considering the influences of the gravity, the Body Force Weighted method is used for pressure interpolation. The velocity gradient on the left inlet side is solved by the Least Squares Cell Based method.

In order to accurately describe the motion responses and loading characteristics of the suspended submersible under the action of ISW. Here, the two coordinate systems are defined which contained the the Earth-fixed coordinate system *E-xyz* and moving coordinate system *O-*$x_0y_0z_0$.[32] As shown in Figure 1, the fixed coordinate system is introduced to describe the translation movement of the submersible while its coordinate system origin called *E* is exactly right on the geometric center of the interface of the two-phase fluid at the velocity entrance. The moving coordinate system is established to describe the hydrodynamic characteristics and rotation movement of the submersible while its coordinate system origin called *O* coincides with the center of gravity of the submersible and always moves with the submersible.

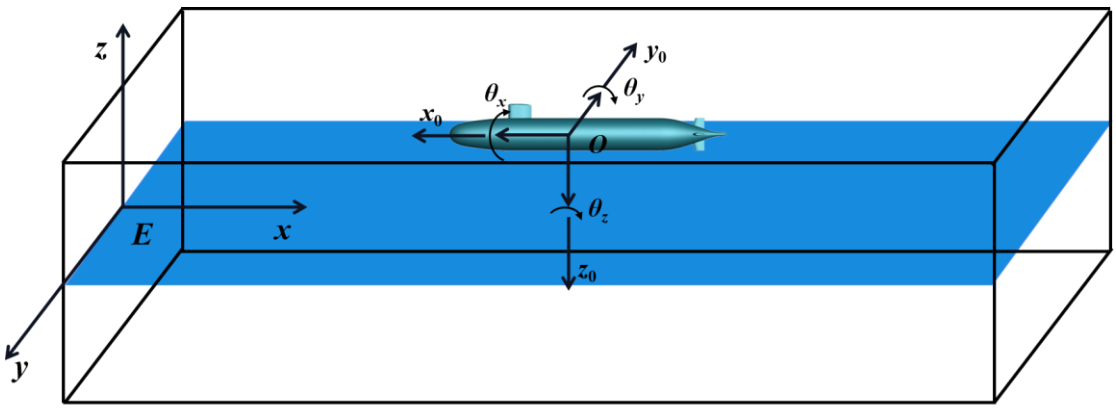

Figure 1. Schematic diagram of the two coordinate systems.

In this paper, the standard operation equations of submersible[33] are introduced to describe the ISW-driven motions of the submersible, and underwater stability of the submersible are fully considered:

 doi:10.20944/preprints202403.0558.v1

$$
\begin{aligned}
&m(\frac{\partial u}{\partial t}+qw-rv)=F_x\\
&m(\frac{\partial v}{\partial t}+ru-pw)=F_y\\
&m(\frac{\partial w}{\partial t}+pv-qu)=F_z\\
&I_{xx}\frac{\partial p}{\partial t}+(I_{zz}-I_{yy})qr=M_x+N_x\\
&I_{yy}\frac{\partial q}{\partial t}+(I_{xx}-I_{zz})rp=M_y+N_y\\
&I_{zz}\frac{\partial r}{\partial t}+(I_{yy}-I_{xx})pq=M_z+N_z
\end{aligned}
\tag{3}
$$

where m is the mass of the submersible, I_{xx},I_{yy},I_{zz} are the rotational inertia of the submersible, u, v, w are the translation velocities of the submersible, p, q, r are the angular velocities of the submersible relative to the moving coordinate system, F_x,F_y,F_z and M_x,M_y,M_z are the fluid field forces and torques applied on the wet surface of submersible by the fluid field, which are obtained by solving the discretized RANS equations on Fluent; As seen in the schematic drawing in Figure 2. N_x,N_y,N_z are the recovery torques of the submersible, derived from the stability of the submersible itself:

$$
\left(N_x,N_y,N_z\right)=mg\Delta h\left(-\sin\theta_x,-\sin\theta_y,0\right),
\tag{4}
$$

where θ_x,θ_y are the turning angles of the submersible in the roll and pitch directions, respectively, and Δh is is the height difference between the center of the gravity ***B*** and the center of the buoyancy ***G***.

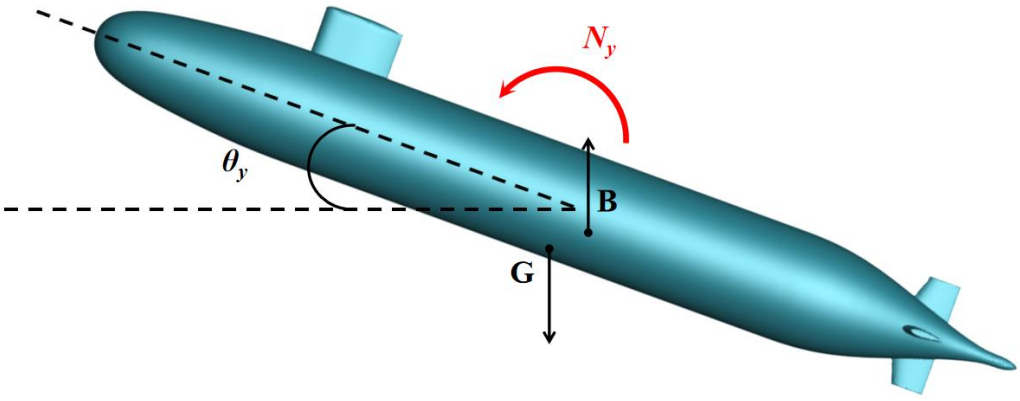

Figure 2. Schematic diagram of the stability of the submersible in the pitch direction.

In order to simulate the FSI process, the interface between ISW fluid field and movable submersible is established based on the secondary development of Fluent to achieve the numerical information exchange.[34] The numerical implementation method of the FSI interface is to write the user defined function (UDF) combined with the overset dynamic mesh method. The specific fluid-structure interaction process is shown as follows in Figure 3: The generation and propagation of ISW is simulated in numerical wave tank based on the ISW equations, and dispersed RANS equations are solved to obtain the hydrodynamic loadings on the submersible in Fluent. Volume Of Fluid (VOF) method is introduced to capture the generation and evolution of ISW interface.[35] Then the motion responses of the submersible can be calculated by introducing the hydrodynamic loadings acting on the wet surface into the standard motion equation of submersible. Based on the overset dynamic mesh method, the wall boundary of the submersible is updated according to the numerical calculated

 doi:10.20944/preprints202403.0558.v1

results, thus, the influence of motions of the structure to the fluid filed can be considered. The aforementioned process is repeated until the all fluid-structure calculation completes.

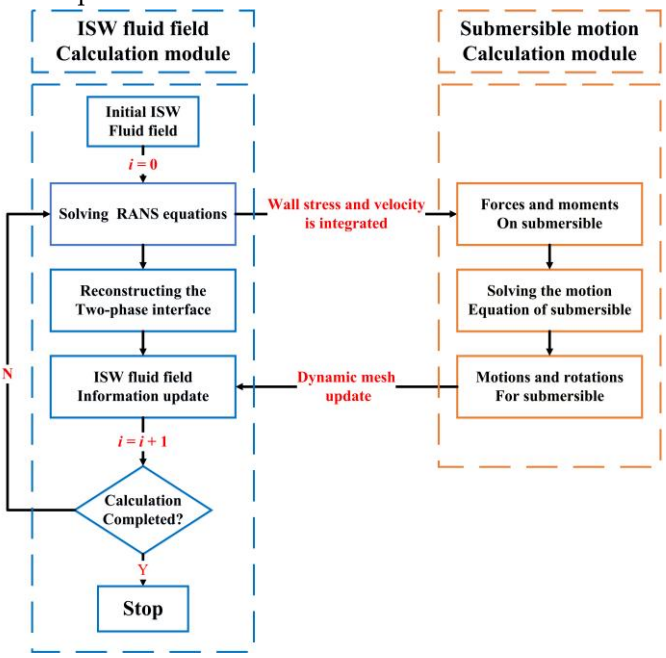

Figure 3. Flow chart of the computational process of the fluid-structure interaction.

2.2. Theory of Internal Solitary Wave

To simplify the numerical solving process below, the actual continuous layer density structure of ocean can be assumed as a fluid with two uniform density layers system.[36] As shown in Figure 4, the densities of the upper and lower layer are ρ_1 and ρ_2 , respectively. The depths of the upper and lower layer are h_1 and h_2 , respectively. The fluid interface between the upper and lower fluid layers is treated as the pycnocline. The top boundary side follows the rigid lid assumption while the bottom boundary is set as no slip wall.

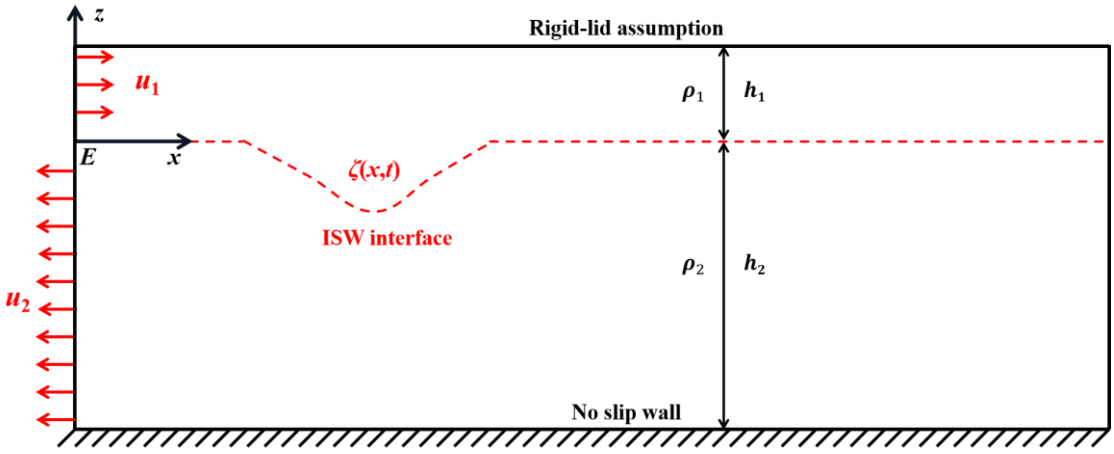

Figure 4. Schematic diagram of ISW numerical tank in assuming as a two-layer fluid.

There are multifarious numerical theories to describe the ISW, different equations are suitable to simulate the generation of ISW for different depth ratios $h_1/h_2$and different amplitudes ξ_0. The eKdV equation[37] is suit to describe ISW with middle nonlinear amplitude, this paper employs the eKdV equation to initialize the ISW fluid field. The interface displacement of ISW can be expressed as follows:

 doi:10.20944/preprints202403.0558.v1

$$\begin{aligned}
&\frac{\partial \zeta}{\partial t}+c_0\frac{\partial \zeta}{\partial x}+c_1\zeta\frac{\partial \zeta}{\partial x}+c_2\frac{\partial^3 \zeta}{\partial x^3}+c_3\zeta^2\frac{\partial \zeta}{\partial x}=0,\\
&c_0^2=gh_1h_2\left(\rho_2-\rho_1\right)/\left(\rho_1h_2+\rho_2h_1\right),\\
&c_1=-3c_0\left(\rho_1h_2^2-\rho_2h_1^2\right)/\left[2\left(\rho_1h_1h_2^2+\rho_2h_1^2h_2\right)\right],\\
&c_2=c_0\left(\rho_2h_1h_2^2+\rho_1h_1^2h_2\right)/\left[6\left(\rho_1h_2+\rho_2h_1\right)\right],\\
&c_3=\frac{3c_0}{h_1^2h_2^2}\left(\frac{7}{8}\left(\frac{\rho_1h_2^2-\rho_2h_1^2}{\rho_1h_2+\rho_2h_1}\right)^2-\frac{\rho_1h_2^3+\rho_2h_1^3}{\rho_1h_2+\rho_2h_1}\right),
\end{aligned} \tag{5}$$

where ξ denotes the wave profile of ISW, the analytical solution of $\xi(x,t)$ is

$$\begin{aligned}
&\zeta(x,t)=\zeta_0/\left[B+(1-B)\cosh^2\left(\left(x-c_{eKdV}t\right)/\lambda_{eKdV}\right)\right],\\
&B=-c_3\zeta_0/\left(2c_1+c_3\zeta_0\right),
\end{aligned} \tag{6}$$

Its phase velocity c_{eKdV} and characteristic wave length λ_{eKdV} are

$$c_{eKdV}=c_0+\zeta_0\left(c_1+c_3\zeta_0/2\right)/3, \tag{7}$$

$$\lambda_{eKdV}=\sqrt{12c_2/\left[\left(c_1+c_3\zeta_0/2\right)\zeta_0\right]}, \tag{8}$$

Numerical simulation of ISW is carried out by solving the eKdV equation and enforced the velocity distribution condition on the inlet flow boundary. The upper layer and lower layer velocity can be derived from the ISW profiles, respectively.[38] The induced velocity of the upper layer and lower layer fluid u_1 and u_2 are

$$u_i=(-1)^i\frac{c_{eKdV}\zeta_0}{h_i},\ \text{where } i=1,2 \tag{9}$$

3. Modeling and Validations

3.1. ISW Numerical Tank and Submersible Model

In this paper, the standard submersible model proposed by Defense Advanced Research Projects Agency (DARPA) called Suboff [39,40] is introduced to investigate the fluid-structure interaction effect between ISW fluid field and movable submersible. The total length and the maximum diameter of the submersible model are $L_{pp}=4.356m$ and $D=0.508m$. The volume of displacement of the submersible is $V=0.705m^3$and the height difference between the gravity center and the buoyancy center is $\Delta h=0.0162m$. The schematic diagram of the interaction numerical model is given in Figure 5. The length of the wave tank is $L=150m$, while its width and height are taken as $B=15m$ and $H=20m$, respectively. The head of the submersible is oriented toward the propagation direction of ISW, and the initial location of the submersible is 50 m away from the velocity inlet boundary.

Preprints.org (www.preprints.org) | NOT PEER-REVIEWED | Posted: 11 March 2024 doi:10.20944/preprints202403.0558.v1

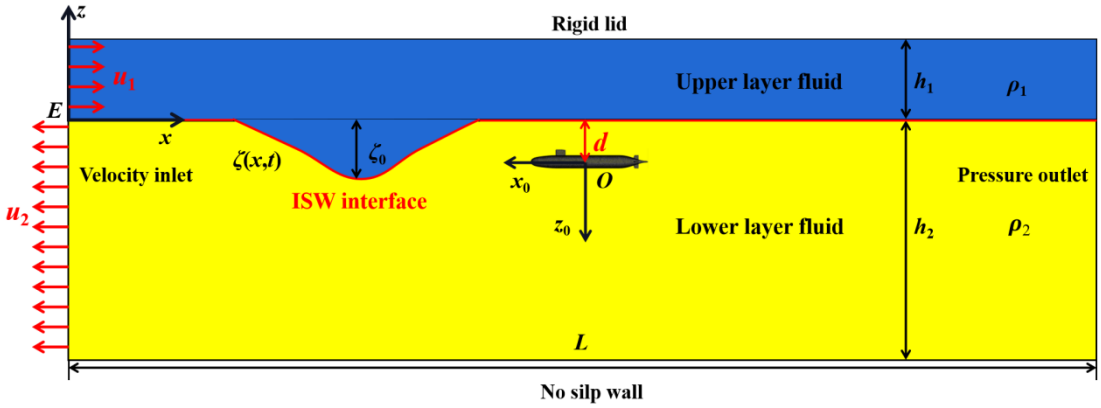

Figure 5. Schematic diagram of the interaction numerical model between ISW and submersible.

For the numerical wave-generation tank, the depths of the upper and lower fluid layers are $h_1 = 5m$ and $h_2 = 15m$, respectively, the densities of the upper and lower fluid layers are $\rho_1 = 998kg/m^3$ and $\rho_2 = 1025kg/m^3$, respectively. The amplitude of the ISW is set as $\xi_0 = -3m$. The initial submerged depth of the submersible called d is defined to describe the relative vertical distance between the initial position of the submersible and the ISW interface. At the initial moment, while the submersible is above the ISW interface, $d > 0$; while the submersible is exactly at the center of the fluid interface, $d = 0$; while the submersible is below the fluid interface, $d < 0$. In order to ensure that the submersible could suspend in the fluid field stably, the density of the submersible body is modified to be consistent with that of the fluid field. The top side of the numerical tank is defined as the symmetrical boundary according to the rigid lid assumption. The left and right boundaries are allocated as the velocity inlet boundary and the pressure outlet boundary, respectively. The surface of the submersible and the bottom of the numerical wave tank are both defined as the wall boundary, while the front and back boundaries are both defined as the symmetrical boundary.

This paper aims to investigate the interaction effect between the movable submersible and ISW fluid field, the overset dynamic mesh method is introduced to consider the large amplitude motions of the suspended submersible which can guarantee the nearby grids to remain free from distortion during the motion[41]. As Figure 6 shown, the whole component domain grid is divided into two parts: foreground grid marked in red and background grid marked in blue. The background region is meshed by the structured grid while the foreground region is meshed by the unstructured polyhedral grid. The foreground grid is meshed refinement near the surface of the submersible which can calculate the hydrodynamic loadings and motions of the submersible more accurately. In order to capture the ISW surface more accurately, the background grid is also partially meshed refinement near the ISW surface. Besides, the foreground region is set as the dynamic mesh component to simulate the ISW-driven motions of the submersible while the background region is set as fixed. The overset interface is constructed to transfer the fluid field information between the movable structure and background fluid field through the method of interpolation. The overset mesh size should be approximately the same as the nearby background mesh size to ensure the quality of the interpolation.

 doi:10.20944/preprints202403.0558.v1

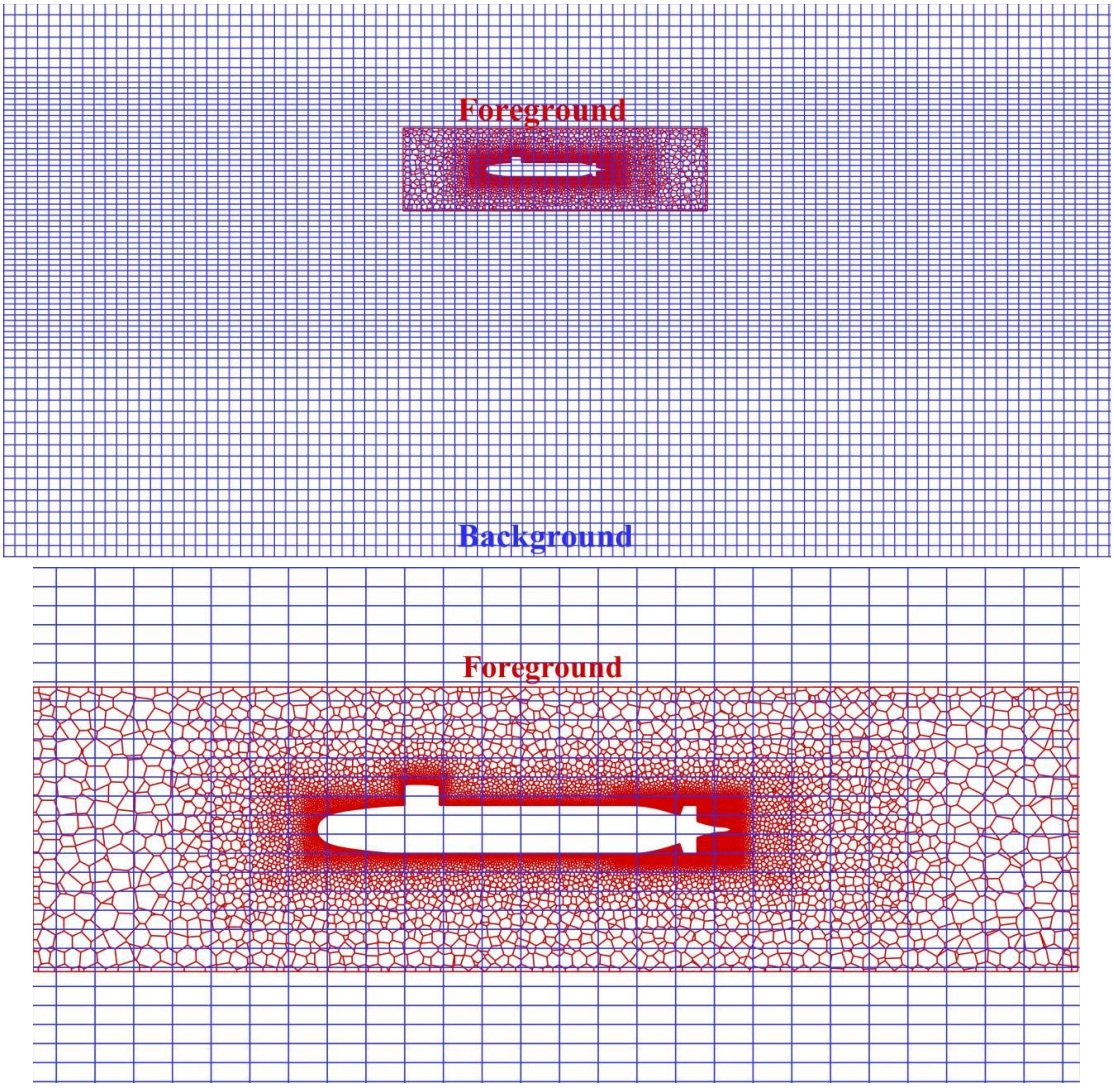

Figure 6. Sketch and mesh of the computational domain.

3.2. Numerical Validations

To test the grid and time step independence of the conducted numerical model, three different foreground grid sizes (i.e, 0.04, 0.02, and 0.01 m) and three different time steps (i.e, 0.04, 0.02, and 0.01s) are adopted to simulate the resistances of the submersible under the current of 17.75 *kn*. As shown in Figure 7, the results indicate that the grid size of 0.02 m and the time step of 0.02 s is accurate enough for the further research. Table 1 gives the comparison of the resistances of the submersible under different velocities obtained by the numerical method and the experimental method, the relative error between the experimental results [40] and the numerical results is less than 1%, the numerical model can precisely simulate the loadings of the structure.

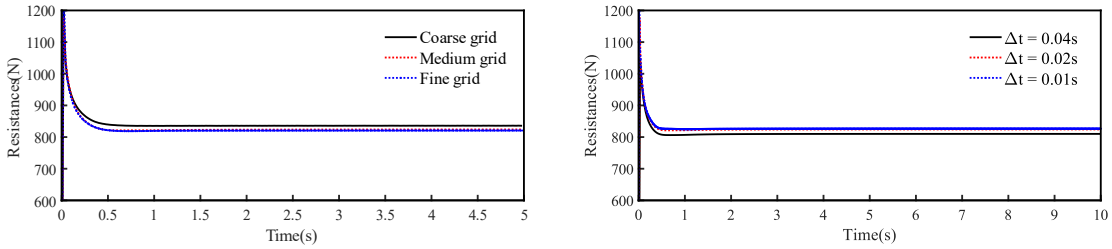

Preprints.org (www.preprints.org) | NOT PEER-REVIEWED | Posted: 11 March 2024 doi:10.20944/preprints202403.0558.v1

Figure 7. Grid size and time step independence validation results. Left: Comparison of the submersible resistances at different mesh size of foreground region, Right: Comparison of the submersible resistances at different time steps.

Table 1. Comparison of the resistances between the numerical result and experiment result.

Velocity(kn)	Numerical Results (N)	Experimental Results (N)	Relative Error (%)
10	282	284	-0.704
11.85	387	389	-0.514
13.92	526	527	-0.190
16	680	676	0.592
17.79	827	821	0.731

To validate the accuracy of the ISW generation method, we simulate the generation and propagation of the ISW and record the time history of the ISW interface and the vertical distribution of the horizontal velocity. As shown in Figure 8, good agreements were achieved by comparing with numerical result and theoretical solution of the eKdV equation. Moreover, the ISW field and loadings of the underwater structure have been further validated by comparing with experimental data in the last published article[28].

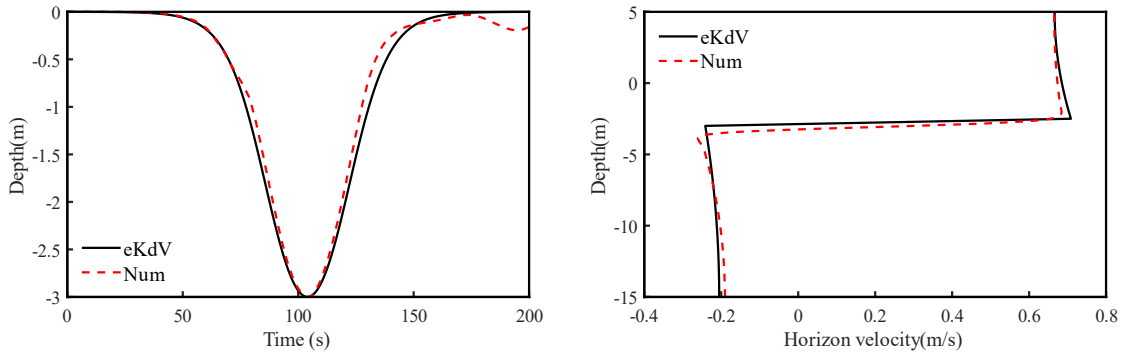

Figure 8. Comparison of the ISW interface time history and the vertical distribution of the horizon velocity of the ISW fluid field between the eKdV theory and the numerical simulation. Left: ISW interface time history, Right: Vertical distribution of the horizon velocity in the ISW fluid field.

In order to further validate the reliability of the motion simulation of the underwater structure under the action of ISW, the numerical simulation was conducted and compared with the experimental data of Cui et al [14]. As shown in Figure 9, the length, width and height of the numerical tank are 15m, 0.4m and 0.5m, respectively, and the depth of the upper and lower fluid layers are 0.15m and 0.35m, respectively. The density of upper fluid and lower fluid are $\rho_1 = 998kg/m^3$and $\rho_2 = 1015kg/m^3$, respectively, and the amplitude of ISW is $\xi_0 = -6$ cm. The length and diameter of the underwater slender body structure are $l = 29.8$ cm and $d = 8$ cm, respectively. The slender body is placed at the center of the pycnocline which is 5m far from the wave-generation boundary. Figure 10 shows the comparison between the calculated motions and experimental data. The numerical results are in good agreement with the experimental results which illustrates that the present numerical model is accurate enough to simulate the motions of the underwater structure under ISW fluid field.

 doi:10.20944/preprints202403.0558.v1

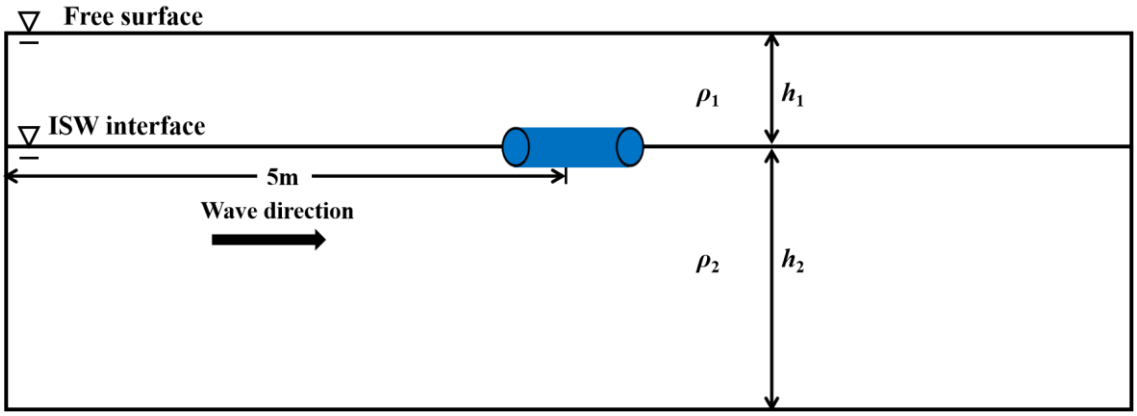

Figure 9. Sketch of validation case on the motions of underwater cylinder in ISW environment.

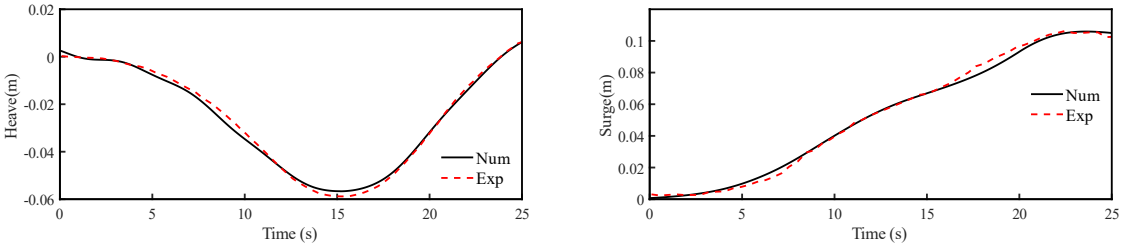

Figure 10. Comparison of motion responses of the submerged cylinder in ISW field between numerical result and experimental result. Left: the heave motion. Right: the surge motion.

4. Results and Discussions

Due to the strong effect of the ISW fluid field, the the motion trajectory of the submersible would be greatly disturbed, the submersible moves up and down during the whole process. In this section, the motion characteristic of the suspended submersible under ISW is investigated, and the influence of the initial submerged depth of the submersible d and the wave amplitude of ISW ξ_0 on the interaction effect is fully discussed. In order to simplify the numerical case analysis below, the relevant physical quantities such as submerged depth and motions of the structure are converted to dimensionless form by the following expression:

$$X^* = \frac{X}{H}, Y^* = \frac{Y}{H}, Z^* = \frac{Z}{H}$$
$$\zeta_0^* = \frac{\zeta_0}{H}, d^* = \frac{d}{H} \tag{10}$$

The dimensionless variables are introduced with a mark *, X, Y and Z indicate the surge, sway and heave motions of the submersible, respectively.

4.1. Dynamic Responses of the Suspended Submersible under ISW

In this section, the numerical simulation is conducted to investigate the dynamic interaction characteristic of the submersible under ISW fluid field. The suspended submersible is placed at the upper layer fluid ($d^* = 0.05$) and the amplitude of ISW is set as $\xi_0^* = -0.15$, other parameters are the same as Sec. 3.1. Figure 11 gives the whole interaction process between the movable submersible and ISW surface through the velocity vector contours. It can be observed that the motions of the submersible are always dominated by the internal wave fluid field. As the ISW surface propagates near or away from the submersible in the horizontal direction, the submersible moves down firstly and then moves up quickly.

Preprints.org (www.preprints.org) | NOT PEER-REVIEWED | Posted: 11 March 2024 doi:10.20944/preprints202403.0558.v1

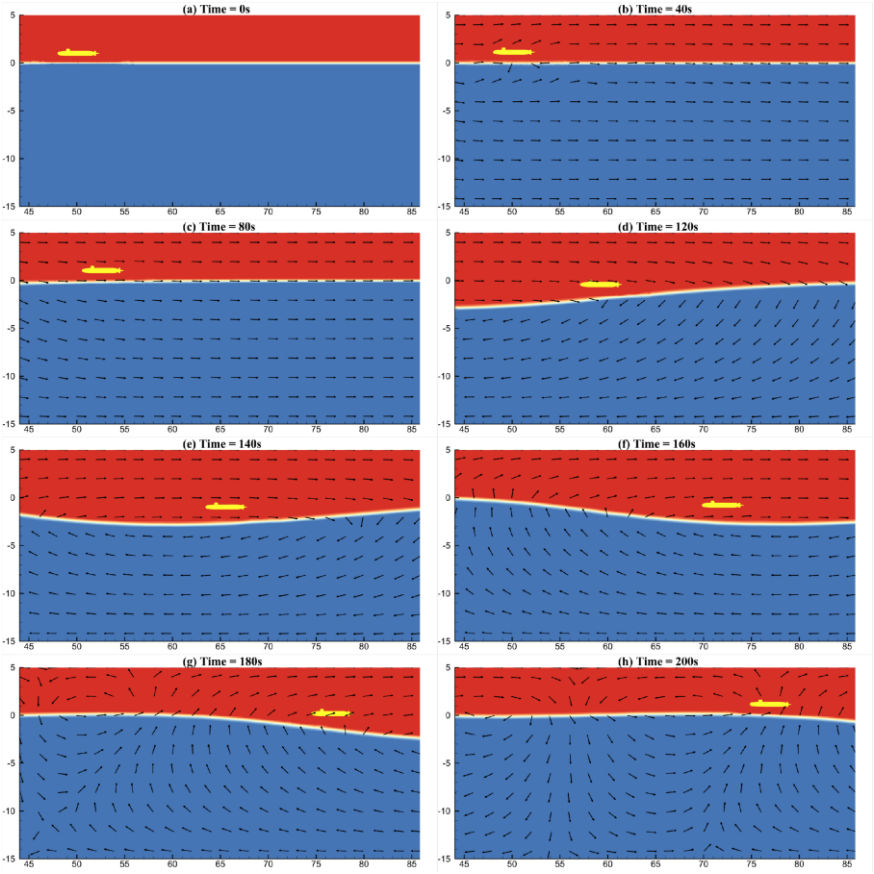

Figure 11. The velocity vector contours of the interaction process between the movable submersible and ISW surface at typical moments.

Figure 12 shows the time history of the motion responses of the suspended submersible located at upper layer fluid ($d^* = 0.05$). In order to describe the interaction process more conveniently, the whole interaction process is divided into three stages according to the amplitude of the heave motion which marked as I, II, III in Figure 12. The two adjacent stages are separated by vertical black dashed lines. Stage. I (0s-80s), the ISW propagates forwards and gradually approaches the submersible, the submersible moves slowly driven by the ISW fluid field; Stage. II (80s-140s), the submersible dives to the maximum submerged depth under the action of the internal wave fluid field while the submersible moves along the direction of the ISW propagation; Stage. III (140s-200s), the submersible quickly floats to the initial suspended surface while the submersible moves to the positive amplitude and then moves backward for a short distance in the horizontal direction.

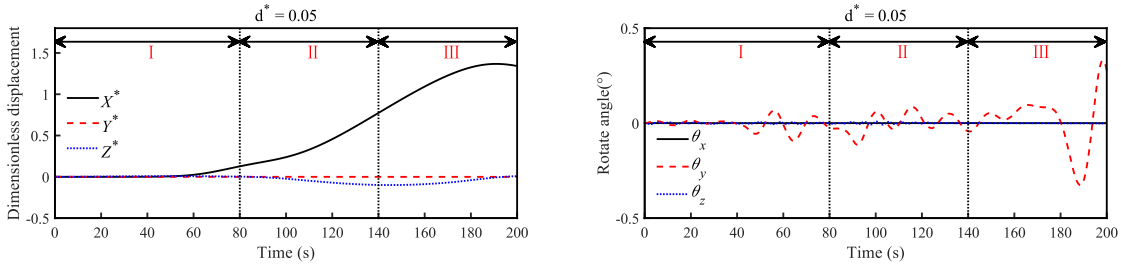

Figure 12. Time history of motion responses of the suspended submersible subject to ISW.

Under the guidance of the ISW fluid field, the suspended submersible moves and its moving speed changes with the relative horizontal distance to the ISW surface. While the submersible is far from the wave surface, the motion speed is relatively low. By contrast, while ISW surface propagates

 doi:10.20944/preprints202403.0558.v1

to close to the submersible, the submersible will be strongly disturbed by the core fluid field, and its moving speed will increase significantly. Due to the high horizontal velocity of the ISW fluid field, the driven motion of the suspended submersible in the horizontal direction is most significant. Moreover, the propagation phase velocity of the ISW is much larger than the horizontal moving velocity of the submersible, the submersible stops moving and does not continue to follow the fluid field of ISW after moving for a certain distance along the positive propagation direction of the ISW.

In the vertical direction, at the first two stages, the ISW propagates forwards and gradually approaches the submersible. Under the action of ISW fluid field near the right side of the wave surface, the submersible continues to dive, and its diving speed increases as the ISW surface approaches the submersible, Figure 11 (a) - Figure 11 (e) shows the diving process of the submersible. The submersible reaches its dropping amplitude at the end of the stage. II (Time=140s), as shown in Figure 11 (e), at this time, the submersible is just located above the trough of ISW. Therefore, the dropping amplitude of the submersible is less than the wave amplitude of ISW. At stage. III, as shown in Figure 11(f) - Figure 11 (h), the submersible quickly moves up and returns to the initial suspended surface under action of the fluid field near the left wave surface.

In the pitch direction, the pitch angle of the submersible θ_y has hardly changed at the first two stages, and only generates a small angle which is less than 0.5° under the influence of the fluctuation of the tail wave at stage. III, as shown in Figure 11(h). It is also noted that the motion responses of the submersible in other three directions are not significant because the ISW approximates a two-dimensional wave.

The motion of the suspended submersible is almost dominated by the ISW fluid field during the whole process. Figure 13 shows the overall motion trajectory of the suspended submersible located at the upper layer fluid. The suspended submersible floats or dives with the fluctuation of the wave surface and its motion trajectory resembles a counterclockwise semi ellipse. The motion amplitude of the submersible in the x direction is nearly 14 times larger than that in the z direction. And the initial point and ended point of the motion trajectory are almost on the same vertical plane. It is also worth noticing that the submersible always moves in the upper layer fluid medium and never penetrates the wave surface during the whole process. The submersible only moves to be close to or far from the wave surface under the fluid field in the vertical direction. It can be seen from Figure 14, the submersible moves vertically away from the wave surface at stage. II and approaches the wave surface at stage. III.

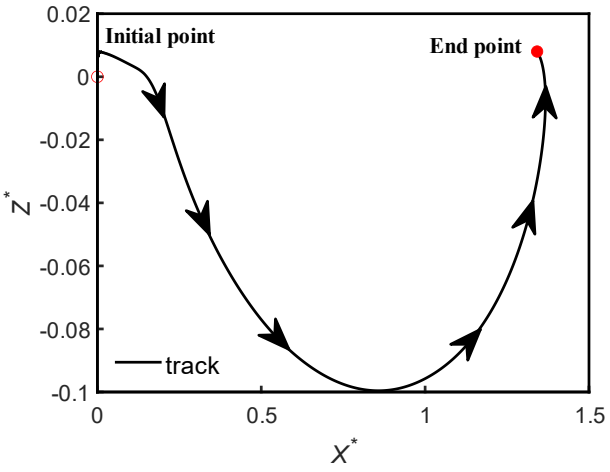

Figure 13. Motion trajectory of the suspended submersible located at upper layer under ISW.

Preprints.org (www.preprints.org) | NOT PEER-REVIEWED | Posted: 11 March 2024 doi:10.20944/preprints202403.0558.v1

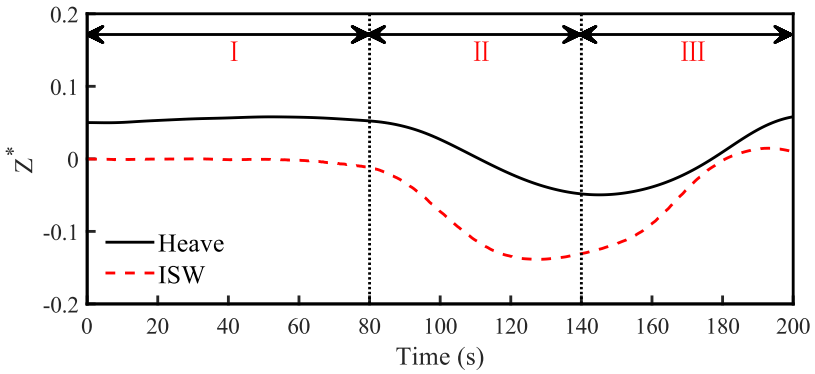

Figure 14. The relative motion of submersible to the ISW surface in the vertical direction.

In order to illustrate the effect of the recovery moments of the submersible on ensuring the stability of the attitude of submersible. Another case whose recovery moments is set as $N(N_x, N_y, N_z) = 0$ is simulated. Figure 15 gives the comparisons of the motion responses of the suspended submersible with or without the recovery moments. The surge motions of submersible with the recovery moments is totally equal to that without the recovery moments. In the heave motion, there are slight differences between the submersible with recovery moments and that without recovery moments. However, the roll and pitch motions of the submersible without recovery moments are much larger than that contained with recovery moments. It can be seen that recovery moments play an important role on maintaining the stability of its attitude.

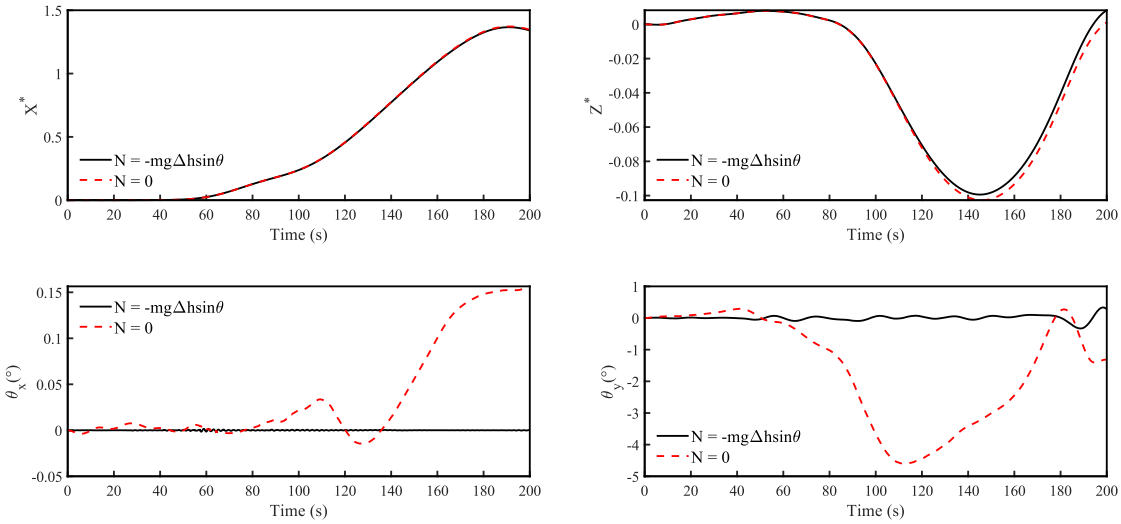

Figure 15. Comparison of motion responses of the suspended submersible with or without the recovery moments in the ISW fluid field.

4.2. The Effect of the Initial Suspended Depth on the Motion Response of the Suspended Submersible

In section 4.1, the interaction characteristics of a suspended submersible located at the upper layer fluid ($d^* = 0.05$) is discussed. The motion behaviors of the submersible at different initial submerged positions are significantly different due to the flow field and density field. In order to explore the effects of the initial depth on the dynamic kinematic properties of the suspended submersible, this section sets eight cases with various initial suspended positions, as shown in Table 2 and Figure 16.

 doi:10.20944/preprints202403.0558.v1

Table 2. Case setups of the relative positions to the wave surface.

Position	Distance to pycnocline (d^*)	Density(kg/m^3)
Upper fluid	0.1	998
	0.05	998
Pycnocline	0	1013
Lower fluid	-0.05	1025
	-0.15	1025
	-0.25	1025
	-0.35	1025
	-0.45	1025

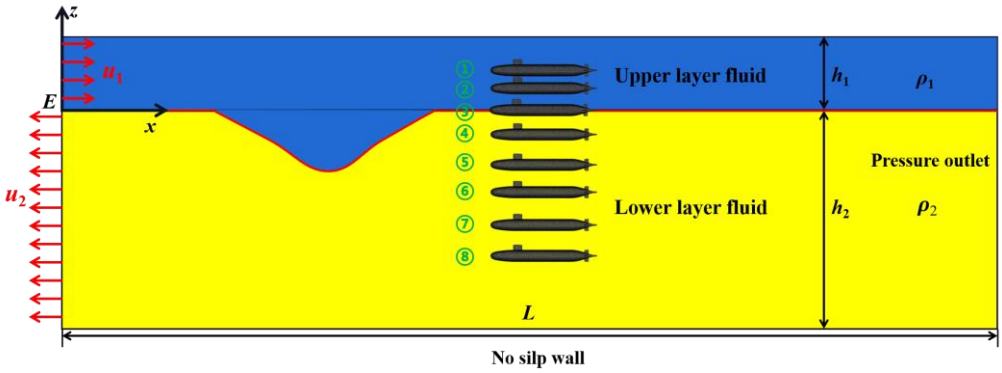

Figure 16. Schematic diagram of interaction between suspended submersible at eight different initial submerged depths and ISW.

Figure 17 gives the velocity vector contours to show the interaction process between the ISW fluid field and the suspended submersible at different initial submerged depths ($d^* = 0.05, 0, -0.05, -0.15$). It can be found that the the vertical motion characteristic of the submersible located at different positions are similar, while the significant differences are existed in longitudinal motion. Moreover, during the whole process, all the submersibles only move in the single medium and do not penetrate the wave surface. Considering the interaction effect between the ISW fluid field and the suspended submersible, in addition to focusing on the induced motions of the submersible under ISW, the interference of the submersible's motion on the ISW fluid field can not be ignored. As shown in Figure 17, the ISW fluid field especially for the wave surface is disturbed by the motions of the submersible, the interference effect of the submersible to the ISW fluid field becomes more significant as the submersible get closed to the wave surface. However, the characteristic length of the submersible L_{pp} is one order of magnitude smaller than the wavelength of the ISW λ_{eKdV}, the interference of the submersible's motion on the ISW fluid field is relatively limited and can usually be ignored in practical physical context. In the laboratory experiment, the scale of the structure is frequently overestimated which may result in some errors.

 doi:10.20944/preprints202403.0558.v1

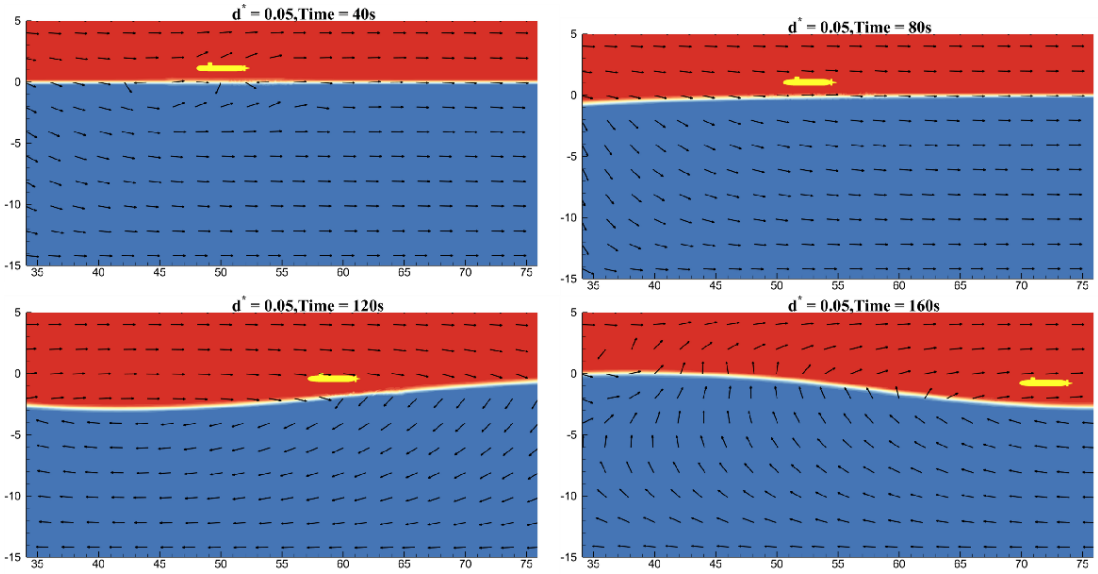

(**a**) The interaction process between the submersible located at lower layer ($d^* = 0.05$) and ISW

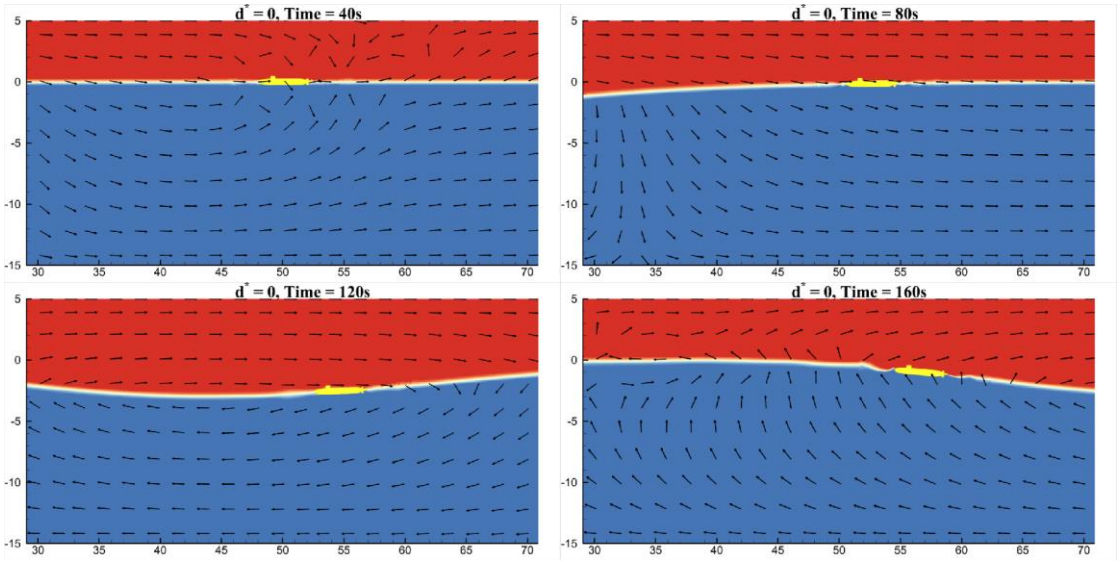

(**b**) The interaction process between the submersible located at ISW surface ($d^* = 0$) and ISW

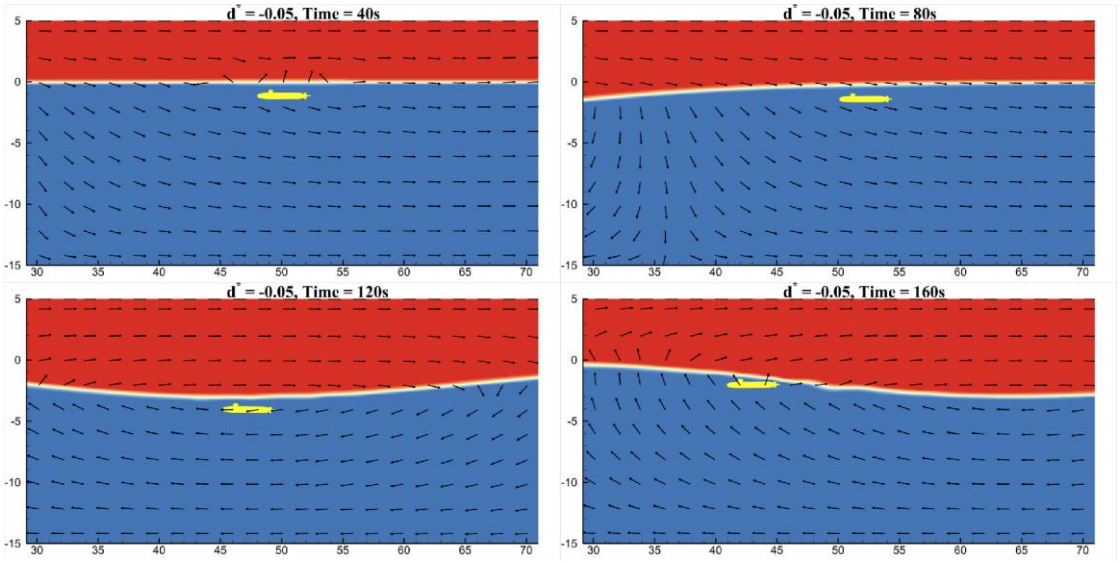

 doi:10.20944/preprints202403.0558.v1

(**c**) The interaction process between the submersible located at lower layer ($d^* = -0.05$) and ISW

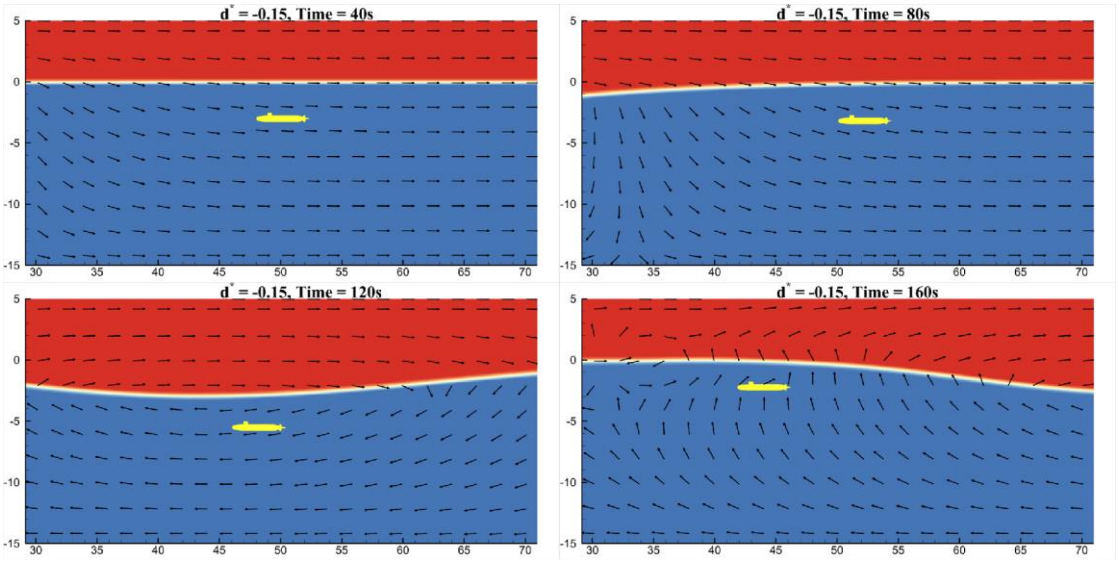

(**d**) The interaction process between the submersible located at lower layer ($d^* = -0.15$) and ISW

Figure 17. The velocity vector contours of interaction between ISW and suspended submersible at different initial submerged depths ($d^* = 0.05, 0, -0.05, -0.15$).

Figure 18 gives the motion responses of the suspended submersible at different submerged depths under the action of ISW with the same wave amplitude ($\xi_0^* = -0.15$). Due to the opposite flow velocity directions between the upper and lower layer fluids, there are significant differences in the longitudinal motion response of the suspended submersible located at the upper and lower layer fluid. When the suspended submersible is located at or above the wave interface ($d^* \geq 0$), the submersible driven by the ISW fluid field moves along the propagation direction of the ISW with significant longitudinal displacements. And the longitudinal motion amplitude of the submersible completely immersed in the upper layer fluid ($d^* > 0$) is much larger than that of the submersible exactly located at the fluid interface ($d^* = 0$); The submersible located below the wave interface ($d^* < 0$) undergoes the significant directional change movement for twice in the longitudinal motion, and the submersible ultimately moves for a certain distance in the opposite direction of the ISW propagation relative to its initial position. Its longitudinal motion amplitude is smaller than that of the submersible located above the wave interface. Besides, for the submersible located at the same fluid medium ($d^* > 0$ or $d^* < 0$), the influence of the initial position of the submersible on the longitudinal motion response is not significant while leaves slight differences in the motion amplitude. Generally speaking, the longitudinal motion amplitude of the submersible decreases with the increase of the distance from the submersible to the pycnocline. And the longitudinal motion characteristic of submersible is consistent with the vertical distribution characteristics of horizontal flow velocity in the internal wave flow field, that is, the horizontal velocity of the flow field decreases with the increase of distance from the interface.

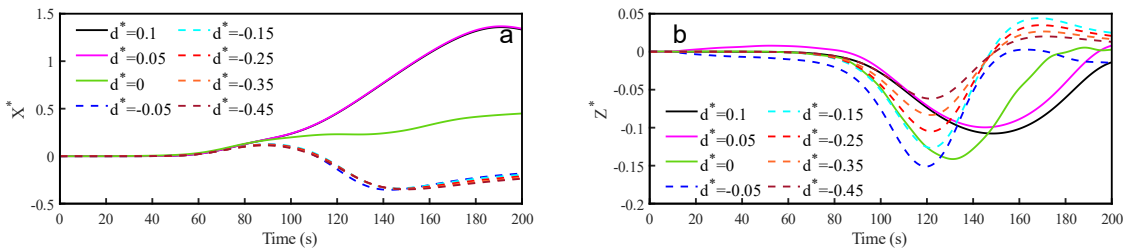

 doi:10.20944/preprints202403.0558.v1

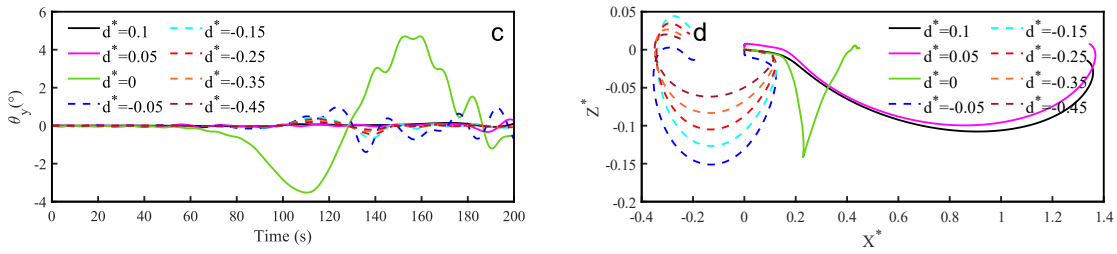

Figure 18. Motion responses of suspended submersible at different initial submerged depths under ISW field ($d^* = 0.1, 0.05, 0, -0.05, -0.15, -0.25, -0.35, -0.45$).(a) Surge motion, (b) heave motion, (c) pitch motion, (d)motion trajectory.

Regarding the heave motion, the motion characteristic of the submersible located at different initial suspended depths is similar. The submersible firstly dives to the amplitude and then quickly floats up. However, the motion process of the suspended submersible located at the different positions in the heave direction still remain some differences, as shown in Figure 18(b). When the suspended submersible dives to the dropping amplitude, the submersible at the wave interface ($d^* = 0$) is located exactly at the trough, the submersible at the upper fluid ($d^* > 0$) is located above the trough while the submersible at the lower fluid interface ($d^* < 0$) is located just below the trough. The vertical motion of the submersible located at the fluid interface ($d^* = 0$) is completely synchronized with the ISW surface. For the submersible located at the same medium ($d^* > 0$ or $d^* < 0$), the amplitude of the dropping depth decreases and the time to reach the amplitude increases with an increase of the distance to the ISW interface. Moreover, the dropping amplitude of the submersible located at the lower layer fluid decreases proportionally with increasing of distance to the wave interface.

Regarding the pitch motion, there are significant differences in the longitudinal inclination angle of the submersibles located at different positions, as shown in Figure 18(c). The pitch motion of the submersible ($d^* = 0$) located at the interface always fluctuates with the ISW surface, and the pitch angle is always equal to the wave inclined angle at the submersible's position, as shown in Figure 17(b). When the submersible dives near the right wave surface, its burial angle increases due to the uneven distribution of the internal forces acting on the surface of the submersible. When the submersible dives to the ISW trough, its pitch angle exactly returns zero degrees. When the submersible floats up on the left wave surface, the bow angle of the submersible increases with wave inclination angle. For the submersible located above the wave interface ($d^* > 0$), there is little change in the pitch angle during the whole process. The submersible located below the wave interface ($d^* < 0$) only generates a small inclination angle while approaching the core fluid field of the ISW, and the amplitude of the inclination angle is less than 3°. Similarly, the amplitude of the longitudinal inclination angle decreases as its relative distance to the wave surface increases.

Figure 18(d) shows the overall motion trajectory of the submersible under the action of internal wave field. The motion trajectory of the submersible located at the lower layer fluid ($d^* < 0$) is exactly the same as the trajectory of the fluid field and its shape like as an unclosed clockwise ellipse. As the submerged depth increases, the longitudinal motion responses of the submersible is not affected, but its vertical motion response decreases proportionally, and its motion trajectory becomes flatter; The trajectory of the submersible located at the interface ($d^* = 0$) is shaped like a "V" shape; The trajectory of the submersible located at the upper fluid ($d^* > 0$) is shaped like a semi ellipse with a large eccentricity rotating counterclockwise.

4.3. The Effect of the Wave Amplitude on the Motion Response of the Suspended Submersible

The ISW fluid field with larger wave amplitude has higher induced flow velocity which may result in the huge threat to underwater vehicles. In order to investigate the effect of the wave amplitude on the motion responses of the suspended submersible, in this section, six cases with three different ISW amplitudes ($\xi_0^* = -0.1, -0.15, -0.2$) for the submersible located at the upper and lower

Preprints.org (www.preprints.org) | NOT PEER-REVIEWED | Posted: 11 March 2024 doi:10.20944/preprints202403.0558.v1

fluid layer ($d^* = 0.05,\ d^* = -0.05$) are set, and the other parameters are the same as the Section 4.1, as shown in Table 3 and Figure 19.

Table 3. Case setups of the submersible and ISW with three different amplitudes.

Position	Distance to pycnocline (d^*)	ISW amplitude (ξ_0^*)
Upper layer fluid	0.05	-0.1 -0.15 -0.2
Lower layer fluid	-0.05	-0.1 -0.15 -0.2

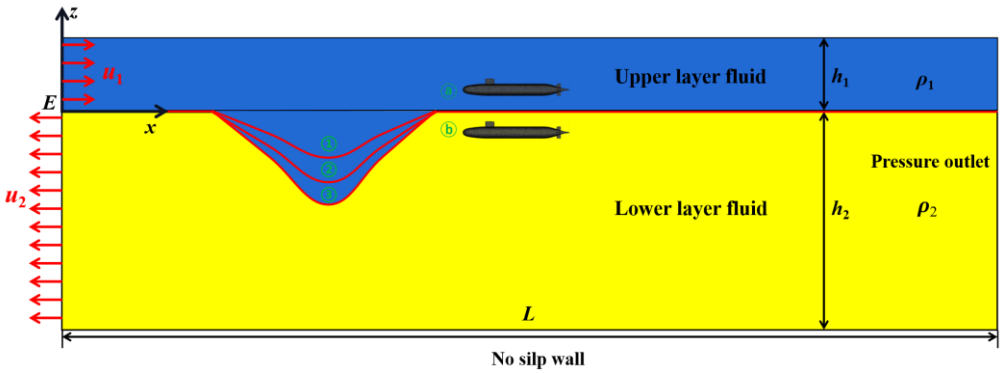

Figure 19. Schematic diagram of interaction between suspended submersible and ISW with different ISW amplitudes($\xi_0^* = -0.1, -0.15, -0.2$).

Figure 20 gives the motion responses of the suspended submersible located at the upper layer fluid ($d^* = 0.05$) and the lower layer fluid ($d^* = -0.05$) under the action of ISW with different ISW amplitudes. The driven motion characteristic of the suspended submersible under ISW at different wave amplitude are similar and only leaves some differences on its motion amplitudes. With an increase in the amplitude of ISW, the motion amplitude of the submersible increases, especially in the surge and heave directions. However, the influence of the ISW amplitude acting on the pitch motion of the submersible is not significant compared with the above mentioned two directions. And the submersible reaches its motion amplitude in the pitch direction while approaches the core fluid field of ISW.

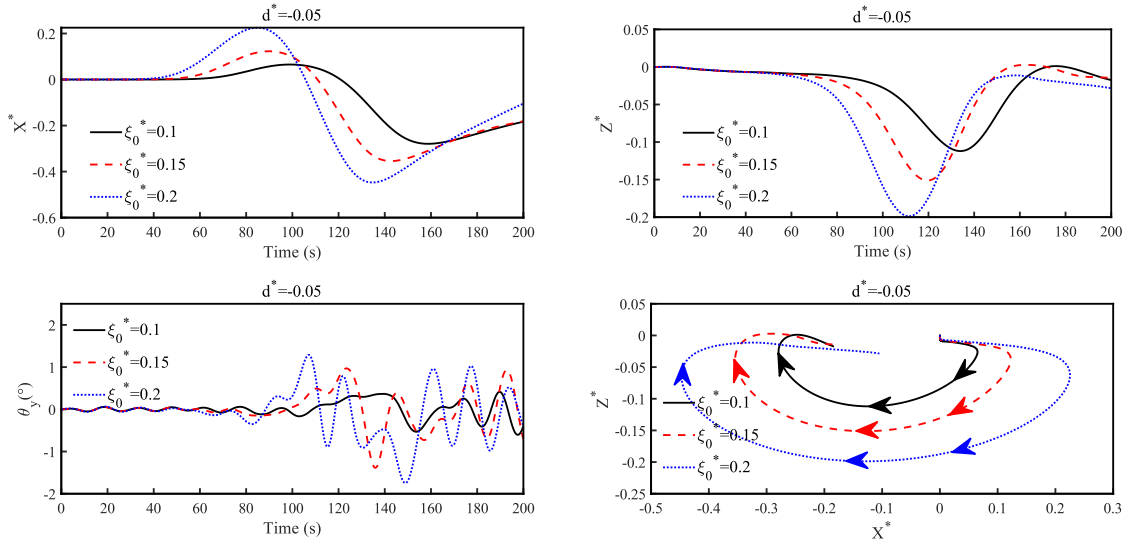

 doi:10.20944/preprints202403.0558.v1

(**a**) The motion responses of the submersible located at lower layer ($d^* = -0.05$) under ISW with different amplitudes.

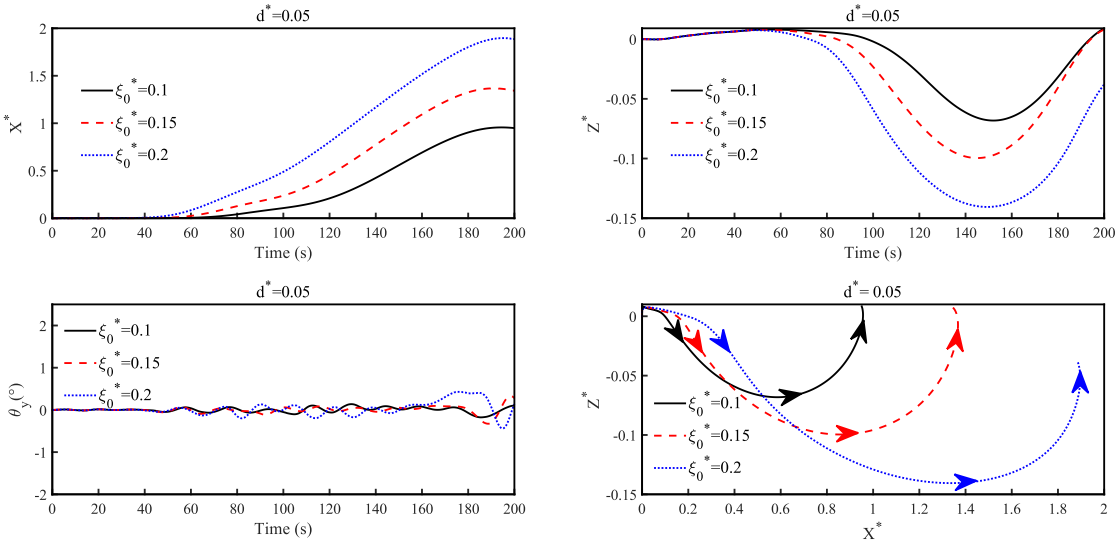

(**b**) The motion responses of the submersible located at upper layer ($d^* = 0.05$) under ISW with different amplitudes.

Figure 20. The motion responses of suspended submersible located at lower layer ($d^* = -0.05$)or upper layer ($d^* = 0.05$)under the ISW at different amplitude($\xi_0^* = -0.1, -0.15, -0.2$).

For the submersible located at the lower layer fluid ($d^* = -0.05$), due to the complexity of the flow field at the lower layer fluid, and the surge motion of the submersible has significant multiple changes. Moreover, the time for the submersible to reach the motion amplitude in the surge and heave directions decreases as the wave amplitude increases. However, for the submersible located at the upper layer fluid ($d^* = 0.05$), with an increase of the wave amplitude, the surge motion is almost completely synchronized and the motion amplitude also increases proportionally.

As shown in Figure 20, the motion trajectory of the submersible located at the upper layer fluid ($d^* = 0.05$) is a clockwise semi ellipse, while the trajectory of the submersible located at the lower fluid ($d^* = -0.05$) shaped like a counterclockwise unclosed ellipse. The ISW amplitude does not change the shape of the submersible's motion trajectory, but only determines the amplitude of its motion trajectory. The range of the motion trajectory is positively correlated with the ISW amplitude in the *x*-*o*-*z* plane.

5. Conclusion

In this paper, a three-dimensional interaction numerical model between the suspended submersible and ISW fluid field is established based on CFD method, and the reliability of the numerical model is welly validated compared with the theoretical solution of eKdV equation and published experimental data. Based on the conducted numerical model, we investigated the dynamic interaction characteristic of the suspended submersible under the action of ISW field. The effects of the initial suspended depth, the ISW amplitude on the motion response of the submersible are also discussed. The conclusions of this paper are drawn as follows:

(1) While the suspended submersible encounters the ISW fluid filed, the motions of the submersible in the *x*-*o*-*z* plane significantly changes. The submersible always drifts with the nearby ISW surface, gradually dives to the amplitude and then floats quickly under the action of the fluid field. During the whole motion process, the submersible does not penetrate the wave surface. Moreover, the change in the pitch angle is not significant due to the action of its own stability.

(2) The initial submerged depth of the submersible is a key factor determining the motion response mode: the submersible located at the wave interface and upper fluid layer ($d^* \geq 0$) continues to

 doi:10.20944/preprints202403.0558.v1

moves for a large distance along the propagation direction of ISW. The motion trajectory of the submersible immersed in the upper layer ($d^* > 0$) is similar to an unclosed clockwise ellipse while that of the submersible at wave interface ($d^* = 0$) is similar to a "V" shape; The submersible located at the lower layer fluid ($d^* < 0$) undergoes directional change movements for twice in the longitudinal direction under the action of the flow field and its motion trajectory shaped like an unclosed ellipse clockwise.

(3) For the submersible located at the same medium ($d^* > 0$ or $d^* < 0$), the longitudinal motion is almost unaffected by its initial suspended depth. However, the amplitude of the surge motion slightly increases with the distance to the interface decreases, which is completely consistent with the vertical distribution characteristics of the horizontal velocity in the ISW flow field; The amplitude of the heave motion decreases as the vertical distance from submersible to the wave interface increases. The submersible located at pycnocline ($d^* = 0$) always adheres to the wave surface, and the inclination angle in the pitch direction changes significantly with the fluctuation of the wave surface.

(4) The amplitude of ISW only influences the planar motion amplitude of the submersible and does not determine its natural motion characteristic. The motion responses of the submersible increase with the increase of the amplitude of ISW. Especially for the heave direction, the amplitude of the submersible even increases proportionally with the increase of the amplitude of ISW. Besides, the influence of amplitude of the ISW acting on the pitch motion of the submersible is not significant.

Author Contributions: Conceptualization, W.J. and H.Z.; methodology, W.J., H.Z. and W.W.; software, H.Z., and W.W.; validation, H.Z.; formal analysis, W.J. and H.Z.; investigation, H.Z.; writing—original draft preparation, H.Z. and W.W.; writing—review and editing, H.Z., W.J. ,W.W.,C.Q.,H.Y.; supervision, W.J., D.L. and W.W.; project administration, W.J. All authors have read and agreed to the published version of the manuscript.

Funding: This research was funded by the National Natural Science Foundation of China (Grant No. 52088102, 51879287, 52271298).

Institutional Review Board Statement: Not applicable.

Informed Consent Statement: Not applicable.

Data Availability Statement: Data is contained within the article.

Conflicts of Interest: The authors declare no conflict of interest.

References

1. Garrett, C., & Munk, W. Internal waves in the ocean. *Annual review of fluid mechanics*, 1979.11(1), 339-369.
2. Osborne, A. R., & Burch, T. L. Internal solitons in the Andaman Sea. *Science*, 1980.208(4443), 451-460.
3. C. Ebbesmeyer, C.A. Coomes, R. Hamilton, et al., New observations on internal waves (solitons) in the South China Sea using an acoustic Doppler current profiler, *Mar. Technol. Soc. J.* 91 (1991) 165–175
4. Vlasenko V, Stashchuk N, Guo C, et al. Multimodal structure of baroclinic tides in the South China Sea. *Nonlinear Processes in Geophysics*, 2010, 17(5): 529-543.
5. Huang,X., Chen,Z., Zhao W, et al. An extreme internal solitary wave event observed in the northern South China Sea. *Sci. Rep*, 2016, 6(1): 30041.
6. Zhang,M., Hu,H.H., Du,P., et al, Detection of an internal solitary wave by the underwater vehicle based on machine learning, *Phys. Fluids* 2022.34(11), 115137.
7. Y. Gong, J. Xie, J. Xu et al, Oceanic ISWs at the Indonesian submersible wreckage site, *Acta Oceanol. Sin* 2022,41, 109-113.
8. Wang, T., Huang, X.D.; Zhao, W.; Zheng, S.H.; Yang, Y.C.; Tian, J.W. Internal Solitary Wave Activities near the Indonesian Submarine Wreck Site Inferred from Satellite Images. *J. Mar. Sci. Eng.* 2022, 10, 197.
9. Chen,M., Chen. K., You. Y. Experimental investigation of internal solitary wave forces on a semi-submersible. *Ocean Eng*, 2017, 141: 205-214.
10. Chen,M., Chen,J., You,Y.X. Forces on a semi-submersible in internal solitary waves with different propagation directions. *Ocean Eng*, 2020, 217: 107864.

11. Cui J, Dong S, Wang Z, et al. Experimental research on internal solitary waves interacting with moored floating structures. *Mar. Struct*, 2019, 67: 102641.
12. Wang S D, Wei G, Du H, et al. Experimental investigation of the wave-flow structure of an oblique internal solitary wave and its force exerted on a slender body. *Ocean Eng*, 2020, 201: 107057.
13. Wang S D, Du H, Wei G, et al. Effects of the inhomogeneous vertical structure of an internal solitary wave on the force exerted on a horizontal transverse cylinder. *Phys. Fluids*, 2023, 35(6).
14. Cui J, Dong S, Wang Z, et al. Kinematic response of submerged structures under the action of internal solitary waves. *Ocean Eng*, 2020, 196: 106814.
15. Cui J, Dong S, Wang Z, et al. Experimental study on motion response of a submersible spherical model under the action of internal solitary wave propagating over a ridge topography. *Ocean Eng*, 2022, 258: 111700.
16. Cai S, Long X, Gan Z. A method to estimate the forces exerted by internal solitons on cylindrical piles. *Ocean Eng*, 2003, 30(5): 673-689.
17. Cai S, Wang S, Long X. A simple estimation of the force exerted by internal solitons on cylindrical piles. *Ocean Eng*, 2006, 33(7): 974-980.
18. Cai S, Long X, Wang S. Forces and torques exerted by internal solitons in shear flows on cylindrical piles. *App Ocean Res*, 2008, 30(1): 72-77.
19. K. Feng, Z. Yao, F. Hu et al, Motion simulation of submersible passing through internal solitary wave, *Chi. J. Hydrodyn*. 37(04), 467-473 (2022).
20. X. Liu, Y. Gou, B. Teng, Research on the Trajectory and Gesture of A Slender Submarine Undergoing Significant Motion Under the Action of Internal Solitary Waves" . *Chi. J. Acta Armamentarii* , 2023, 1-12..
21. M. Liu, G. Wei, Z. Sun, Motion response of a horizontal slender submerged ellipsoid induced by head-on interfacial solitary waves. In Proceedings of the 30th National Hydrodynamics Symposium and the 15th National Hydrodynamics Academic Conference, 2019:247-254.
22. Wang,J. et al. An Iterative Updating Method for Dynamic Responses of a Floating Platform Under Action of Internal Solitary Waves. International Conference on Offshore Mechanics and Arctic Engineering. Vol. 58769. American Society of Mechanical Engineers, 2019.
23. Cheng Si. yuan, et al. The influence of internal solitary wave on semi-submersible platform system including mooring line failure." *Ocean Eng* 258 (2022): 111604.
24. J. Li, Q. Zhang, T. Chen, Numerical Investigation of internal solitary wave forces on submersibles in continuously stratified fluids, *J. Mar. Sci. Eng*. 9(12) 1374 (2021).
25. G. He, H. Xie, Z. Zhang et al, Numerical Investigation of internal solitary wave forces on a moving submersible, *J. Mar. Sci. Eng*. 10(8), 1020 (2022).
26. Ding W, Sun H, Zhao X, et al. Numerical study of the interaction between an internal solitary wave and a submerged extended cylinder using OpenFOAM. *Ocean Eng*, 2023, 274: 113985.
27. Cheng L, Du P, Hu H, et al. Control of underwater suspended vehicle to avoid 'falling deep' under the influence of internal solitary waves. *Ships and Offshore Structures*, 2023: 1-19.
28. Wang J, He Z, Xie B, et al. Numerical investigation on the interaction between internal solitary wave and self-propelled submersible. *Phys. Fluids*, 2023, 35(10).
29. Wang C, Wang J, Liu Q, et al. Dynamics and "falling deep" mechanism of submerged floating body under internal solitary waves. *Ocean Eng*, 2023, 288: 116058.
30. Chen H C, Patel V C, Ju S. Solutions of Reynolds-averaged Navier-Stokes equations for three-dimensional incompressible flows. " *J. Sci. Comput. Phys*, 1990, 88(2): 305-336.
31. V. Yakhot, S. Orszag, "Renormalization group analysis of turbulence. I. Basic theory," *J. Sci. Comput*. 1(1), 3-51(1986).
32. Wang, Junrong, et al. Dynamic analysis and swing suppression method of a "Mooring-HLC-Cargo" coupled system. *Ocean Eng* 295 (2024): 116840.
33. M. Gertler M, GR. Hagen, Standard equations of motion for submersible simulation, NSRDC Report 2510 (2020).
34. He G, Zhang C, Xie H, et al. The Numerical Simulation of a Submarine Based on a Dynamic Mesh Method. *J. Mar. Sci. Eng*, 2022, 10(10): 1417.
35. Yu, T., Chen, X., Tang, Y., Wang, J., Wang, Y. and Huang, S., 2023. Numerical modelling of wave run-up heights and loads on multi-degree-of-freedom buoy wave energy converters. *Applied. Energy*, 344, p.121255.

 doi:10.20944/preprints202403.0558.v1

36. C. Koop, G. Butle, "An investigation of ISWs in a two-fluid system," *J. Fluid Mech*. 112, 225-251 (1981).
37. T. Kakutani, N. Yamasaki, "Solitary waves on a two-layer fluid," *J. Phys. Soc. Jpn*. 45(2), 674-679 (1978).
38. Kang, X.L.;Wang,J.R.; Xie, B.T.; He,Z.Y.; Numerical Study on the Fluid Structure Interaction of internal Solitary Waves and a Spar-Type FOWT. *J.Ocean.Uni.Chi* 2023,53(04):98-105.
39. N. Groves, T. Huang, M. Chang, Geometric characteristics of DARPA (Defense Advanced Research Projects Agency) SUBOFF models (DTRC model numbers 5470 and 5471), David Taylor Research Center Bethesda MD Ship Hydromechanics Dept (1989).
40. H. Liu and T. Huang, Summary of DARPA SUBOFF experimental program data, Naval Surface Warfare Center Carderock Div Bethesda MD Hydromechanics Directorate (1998).
41. Sukas O F, Kinaci O K, Cakici F, et al. Hydrodynamic assessment of planing hulls using overset grids. *Appl Ocean Res*, 2017, 65: 35-46.